Granular Matter (2017) 19:36
DOI 10.1007/s10035-017-0720-y

ORIGINAL PAPER

Evaluation of energy contributions using inter-particle forces in granular materials under impact loading

N. Karanjgaokar[1]

Received: 12 October 2016 / Published online: 13 April 2017

Abstract A drop-tower based experimental setup was developed for the impact testing of 2D assembly of cylinders with impactor velocity of around 6 m/s. This drop tower setup was used to load 2D granular assemblies of polyurethane and polycarbonate cylinders of 1″–1.25″ length with three different diameters of 1/4″, 3/8″ and 1/2″. A high speed camera was used for recording the images at speeds between 10,000 and 55,000 fps to monitor the deformation of the cylinders. Kinematic and strain fields in individual grains during each experiment were measured using digital image correlation. These experimentally measured strain and kinematic fields were used as inputs for the granular element method (GEM) based force inference technique and the inter-particle forces in normal and tangential direction were determined at every contact in each experiment. The inter-particle forces at each contact can facilitate the calculation of frictional work done at each contact. The GEM based inter-particle forces for a simple 2 particle granular assembly were found to be in good agreement with predictions from ABAQUS explicit based FEM simulation. The influence of different model parameters was also characterized such as grain stiffness, frictional coefficient was investigated qualitatively. The impact response of the various ordered granular assemblies was also investigated using the GEM approach and the effect of local defects such as voids or layering of granular materials on the wave propagation phenomena is also studied. The presence of the point or line defects have significant effects on the wave propagation in the granular assemblies due to wave scattering and attenuation.

✉ N. Karanjgaokar
nkaranjgaokar@wpi.edu

[1] Mechanical Engineering Department, Worcester Polytechnic Institute, 100 Institute Rd, Worcester, MA 01609-2280, USA

Keywords Energy conservation · Granular media · Low velocity impact · Drop tower · Granular element method · Friction

1 Introduction

Granular materials are conglomerations of discrete solid grains which in its dry state, lack of cohesion and transmit forces via inter-granular contacts through rigid elastic interactions. There can be a wide variation of configurations in a granular assembly owing to the differences in shape and size of individual grains and the packing of the grains in the granular media. This heterogeneous fabric of granular media results in preferred paths for the force transfer in these materials. These preferred pathways results in formation of force chains in dry granular materials as evidenced by numerous experimental studies [1–6] and numerical simulations [3,7–12]. The macroscopic behavior of granular materials has been commonly described using continuum mechanics and phenomenological elastoplasticity [13–17] and hypoplasticity [18,19]. While these models are very successful in engineering applications, they struggle to predict some observable features in the heterogeneous deformation of granular materials.

These inter-particle force networks have tremendous implications on the macroscopic behavior of granular media. The inter-particle forces have been linked to constitutive response [3,6,20–23], wave motion [5,24,25] and energy dissipation [26–28] and also influence phenomenon like jamming [29–31], intruder dynamics [10,32,33] etc. There is a clear need for understanding the connection between microscopic and macroscopic response of granular materials and this missing link is critical to the success of number of defense and industrial applications as shock attenuators, blast mitiga-

tion structures, wave tailoring devices and vibration isolators [34,35]. Grain scale experiments can help with the validation of emerging modeling techniques such as discrete element method [9–12,27] which embrace the links between inter-particle forces and macroscopic properties.

In the past, photoelasticity based techniques have been used extensively to visualize inter-particle forces in granular media [1–6,20,36]. Although photoelasticity is a useful tool for visualization of inter-particle forces, the choice of materials in these works has to be limited to birefringent grains and they require the knowledge of the boundary conditions and contact laws for quantitative measurement of inter-particle forces. While a number of the limitations of the photoelasticity based force measurement techniques have been addressed, they are still restricted by factors such as particle geometry and assumption of a model for contact forces [37,38]. The recently proposed Granular Element Method (GEM) [39,40] provides a versatile alternative for inter-particle force visualization and quantitative measurement of inter-particle forces. The GEM based technique is limited by the capability of experimental techniques to obtain the granular fabric and full-field displacement fields in individual grains as well as the constitutive material parameters for grains. The utility of the GEM based force visualization approach has been demonstrated for granular media under static and dynamic loads and it presents an interesting opportunity for investigating mechanical response of 3D granular media.

The current paper employs a drop-tower based experimental approach to load an assembly of polyurethane and polycarbonate cylinders and uses high speed imaging to record the deformation process. Digital image correlation is used to obtain the particle kinematics and strain fields in the granular assembly. The experimental measurements like granular kinematics, contact points and strain fields are then used to infer the inter-particle forces using the GEM based approach described in [40]. The mathematical framework of the GEM based approach is presented in the next section. The Sect. 3 of this paper discusses the experimental approach designed for the drop-tower testing of the granular assemblies. The influence of different model parameters on the predictions for inter-particle forces is discussed in the Sect. 4 while experimental results obtained for different granular configuration from the experiments are presented along with some discussion in Sect. 5. The contributions of different components of energy evolves during impact event and the evolution of energy for different cases is also presented in Sect. 5.

2 Mathematical framework for granular element method

The granular element method (GEM) developed in [40], depends on the ability of the experimental techniques to obtain certain quantitative information: (1) granular fabric including particle position and contact locations, (2) strain fields and kinematic data within each grain, (3) constitutive parameters for individual grains and (4) parameters describing the inter-particle friction. These measurements are required as an input for the numerical optimization problem employing a mathematical framework to solve an inverse boundary value problem to obtain the inter-particle forces at each contact.

The technique presented in this work uses grain level strain and kinematic data to facilitate inter-particle force visualization using grain level equations: conservation of linear and angular momentum, force balance between the external forces and average stresses within individual grains and description of friction constraints.

The conservation of linear momentum and angular momentum for any grain p can be expressed as follows;

$$\frac{d}{dt}\left(\int_{V_p} \rho v \, dV\right) = \int_{V_p} \rho b \, dV + \int_{\delta V_p} t \, dS \tag{1}$$

$$\frac{d}{dt}\left(\int_{V_p} x \times \rho v \, dV\right) = \int_{V_p} x \times \rho b \, dV + \int_{\delta V_p} x \times t \, dS \tag{2}$$

where ρ is the particle density, b is the body force, t are surface tractions, v is velocity, and V_p and $\delta V p$ represent deformed grain volumes and surfaces. If the body forces b are ignored, the Eqs. (1) and (2) can be reduced by taking a time derivative and can be expressed in terms of the contact forces f^α acting on the grain p over contact points N_c^p, as

$$\sum_{c=1}^{N_c} f^c = \int_{V_p} \rho a \, dV \tag{3}$$

$$\sum_{c=1}^{N_c} x^c \times f^c = \int_{V_p} x \times \rho a \, dV \tag{4}$$

where x is the position vector for an arbitrary point in the grain as shown in Fig. 1 and a is the acceleration vector at the same point. As seen in Fig. 1, we can express $x = x_p^{cm} + \tilde{x}$ and $a = a_p^{cm} + \tilde{a}$ in terms of the position vector x_p^{cm} and acceleration a_p^{cm} of center of mass for grain p. Using these definitions, the equations are further reduced to

$$\sum_{c=1}^{N_c} f^c = m_p a_p^{cm} \tag{5}$$

$$\sum_{c=1}^{N_c} x^c \times f^c = m_p \left(x_p^{cm} \times a_p^{cm}\right) + \int_{V_p} \rho \, (\tilde{x} \times \tilde{a}) \, dV \tag{6}$$

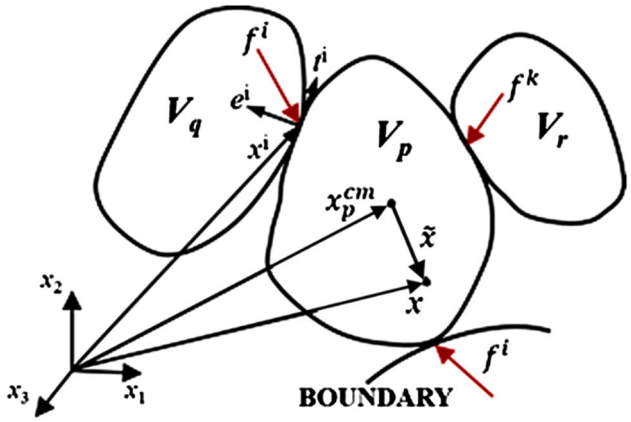

Fig. 1 Illustration of the geometry and kinematics of a contact between grain p and its neighboring grains and domain boundary

where m_p is the mass of each particle. Thus conservation of linear and angular momentum, Eqs. (5) and (6), can be conveniently combined into a single matrix equation for a group of grains in contact as $K_m f = D_m$. The position vector terms on the left hand side of Eq. (6) are grouped together in K_m and the cross-product of acceleration terms on the right hand side of Eq. (6) are grouped together in D_m.

The volume averaged stress tensor '$\bar{\sigma}_p$' in any grain p can be expressed in terms of stress field 'σ' at any point in the grain as;

$$\bar{\sigma}_p = \frac{1}{V_p} \int_{V_p} \sigma \, dV \tag{7}$$

If $\boldsymbol{\sigma}$ within the integral in Eq. (7) is left multiplied by identity matrix $x_{i,k}$ and switching to indicial notation, we can get

$$\bar{\sigma}_{ij} = \frac{1}{V_p} \int_{V_p} \left[\left(x_i \sigma_{kj} \right)_{,k} - x_i \sigma_{kj,k} \right] dV \tag{8}$$

Using divergence theorem on 1st term and balance of linear momentum in absence of body forces gives $\sigma_{kj,k} = \rho a_j$. Thus Eq. (8) can be expressed as

$$\sum_{c=1}^{N_c} x^c \otimes f^c = V_p \bar{\sigma}_p + \int_{V_p} x \otimes \rho a \, dV \tag{9}$$

where $\otimes$ is the dyadic product ($a \otimes b = a_i b_j$). Similar to Eqs. (5) and (6), we can express Eq. (9) in terms of the position vector x_p^{cm} and acceleration a_p^{cm} for center of mass as,

$$\sum_{c=1}^{N_c} x^c \otimes f^c = V_p \bar{\sigma}_p + m_p \left(x_p^{cm} \otimes a_p^{cm} \right) + \int_{V_p} \tilde{x} \otimes \rho \tilde{a} dV \tag{10}$$

The balance of average stress and external forces (Eq. 10) yields 3 equations for each grain. The stress-force balance equations for a group of grains can be combined as a single matrix equation $K_s f = D_s$. The position vector terms on the left hand side of Eq. (10) are grouped together in K_s and the dyadic product of the acceleration terms on the right hand side of Eq. (10) are grouped together in D_s.

A Coulomb type of friction law is used for description of the frictional constraints governing the cohesion-less contact between the grains. The constraints dictate that $-e^i \cdot f^i \geq 0$ and $-\left(e^i \pm \frac{1}{\mu_i} t^i \right) \cdot f^i \geq 0$ for each contact point between grains in the region of interest, where μ_i is the coefficient of friction for each contact. This coefficient of friction can measured from a separate experiment on the materials in granular media and could be dynamic or static depending on the experiment. The cohesion-less force and Coulomb friction constraint equations for the group of grains can be expressed as a matrix equation ($B.\, f \geq 0$) for a group of contacting particles.

Thus the inverse boundary value problem based on this mathematical framework consists of two set of governing equations $K_m f = D_m$ and $K_s f = D_s$, subject to the constraint equation ($B.\, f \geq 0$). Thus the GEM method for obtaining inter-particle forces involves a multi-objective optimization problem of the form,

$$\begin{aligned} f = \arg\min \left(\| K_s f - D_s \|_2 + \lambda \| K_m f - D_m \|_2 \right) \\ \text{subject to: } B.f \geq 0 \end{aligned} \tag{11}$$

Since the magnitude of the errors in stress or momentum is not known, the best strategy is not assign any preference to one set of measurements over the other. Thus we can solve equation 11 for a large range of λ values and obtain a curve of $\| K_s f - D_s \|_2 / \| D_s \|_2$ and $\| K_m f - D_m \|_2 / \| D_m \|_2$. All points on this curve for which neither objective can be decreased without increasing the other are referred to as Pareto optimal points, and the resulting curve is referred to as the optimal trade-off curve or the Pareto front. The optimal 'knee-point' is selected by procedure described in detail in [40], Hurley *et al* have established that this process approximates the knee-point very well in practice. The mass used in Eqs. (6) and (10) must be mass per unit thickness (i.e., actual mass divided by thickness of the particles) and the volume in Eq. (13) must be the area of the face of the particle.

3 Experimental setup and procedure

A schematic for the drop-tower experimental setup used for testing granular assemblies in the current work is shown in Fig. 2a. As seen in the figure, hollow aluminum tube (9' long) is mounted on a rigid load frame and a rigid impactor can free-fall under gravity through the hollow tube. The impactor velocity when it reaches fixture holding the granular assem-

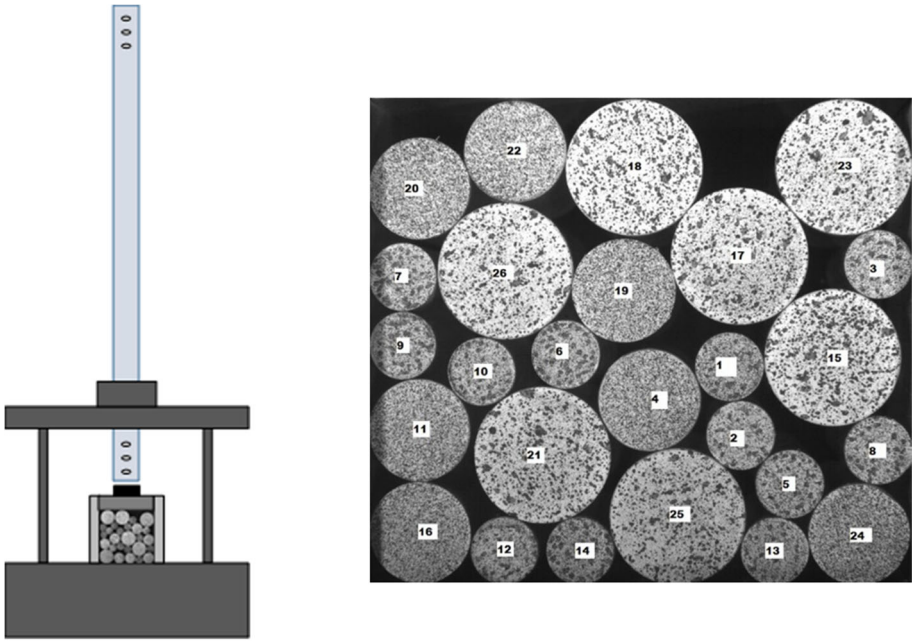

Fig. 2 **a** A schematic representation of the drop tower setup for loading the granular assembly of cylindrical grains, **b** a representative image recorded by the high speed camera for a granular assembly of polyurethane cylindrical grains of three different diameters with speckle-patterns

bly is around 6 m/s. The fixture holding the cylindrical grains has rigid walls on the sides and the bottom face while the slotted top face allows a flat slider to move vertically on impact.

The drop tower setup was used to conduct impact experiments on two different materials: Polyurethane (Durometer 80A) and Impact Resistant Polycarbonate, purchased from McMaster-Carr. For both materials, cylindrical grains with a length of 1.25″ and three different diameters (1/4″, 3/8″ and 1/2″) were arranged as granular assemblies. The detailed alignment procedures are employed to maintain the quasi-2D motion of cylindrical grains during the impact loading. In order to facilitate the use of digital image correlation (DIC), the flat faces of the cylindrical grains were patterned with spray paint with appropriate speckle density for different diameters (see Fig. 2b). The images during the impact experiments were recorded with Phantom v710 high speed camera (resolution between 800 × 800 pixels to 512 × 256 pixels) at frame acquisition rates between 10,000–55,000 fps. The velocity fields from DIC in each grain were then used to calculate the acceleration fields and average accelerations in the grains by numerical differentiation. The recorded images were also used to obtain the position of the centroid and the locations of the particles contacts at each time instant (see Fig. 3a). This was achieved by converting the recorded grayscale image to a binary image and the particle centroids and radius were then detected using a circular Hough transform with MATLAB image processing toolbox. The resulting centroids and radii were then used to find contacting particles: if the distance between two centroids was less than two times the radii of the corresponding particles, the particles were taken to be contacting with appropriate normal and tangent vectors. Similarly, contact points between particles and the boundaries of the fixture were also detected using a MATLAB routine. The DIC software VIC-2D was used to calculate the displacement and velocity fields for each grain separately. The displacement fields were then used to obtain the ε_{xx}, ε_{xy} and ε_{yy} strain fields in each grain (see Fig. 3b–d) and calculate the average strain in each grain. The linear elastic model has assumed for both materials and average strain values can then be used to calculate the average stress values by either assuming plane stress and plane strain.

Noise in the kinematic data (velocity and acceleration) and strain data for each grain was filtered over time using in-built smoothening functions in MATLAB. In the next section, a qualitative investigation of the influence of different assumptions on the inter-particle forces in random granular assembly of polyurethane cylinders using the GEM based approach is presented.

4 Influence of model parameters on GEM results

The analysis in this section is presented for a random arrangement of polyurethane cylinders of 3 different sizes under impact loading. The analysis of the velocity fields obtained from the DIC results for random polyurethane arrangement reveals that although the wave velocity for the polyurethane is around 93 m/s, the wave front moves at approximately 5 m/s through the granular media. The numerical optimization presented in the earlier section links particle positions, accel-

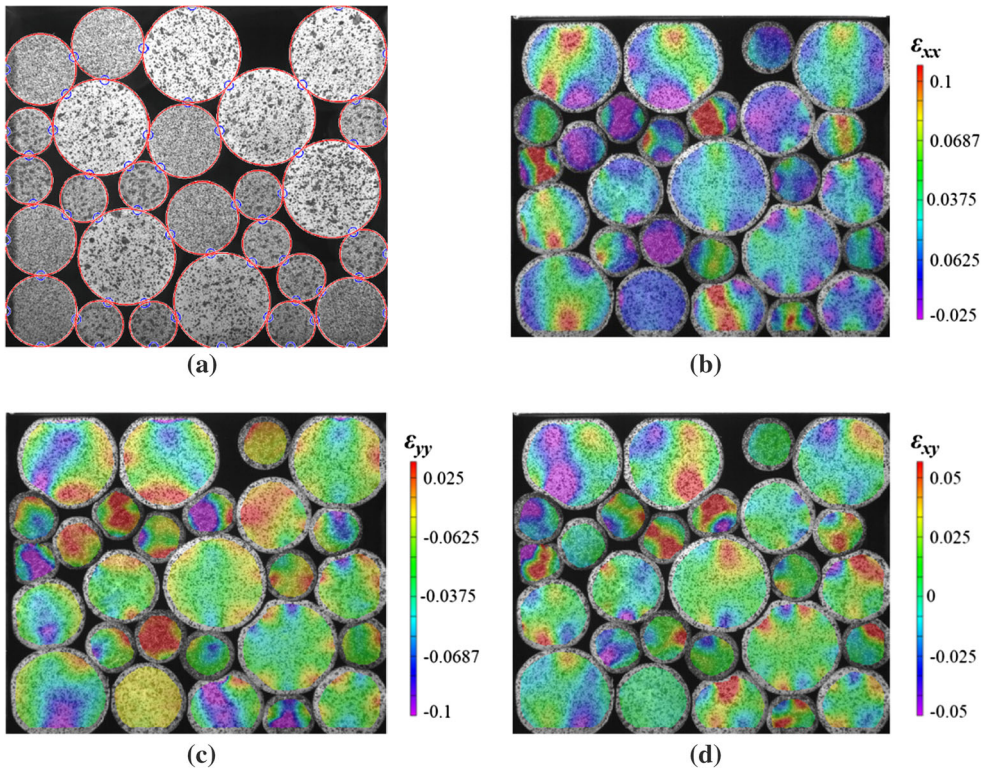

Fig. 3 **a** The particle edges (*red circles*) and contact points (*blue circles*) for a representative image as detected by the circular Hough transform based approach. The **b** ε_{xx}, **c** ε_{yy} and **d** ε_{xy} full-field strain distribution in polyurethane grains during an impact experiment is calculated using Vic-2D at $t = 2$ ms from initial impact (color figure online)

erations, contact points, and stresses to inter-particle forces. Three particle-scale equations accomplish this connection: momentum balance, stress-force relations, and constraint equations. These equations are combined in a multi-objective optimization problem that can be solved to obtain inter-particle forces. The last term in Eqs. (6) and (10) are linked to the local acceleration $\tilde{a}$ and the relative position vector $\tilde{x}$ in the individual grains. In [40], the authors have ignored the effect of local accelerations and have considered only the mean particle acceleration. In the current work, the effect of local acceleration within each grain is investigated and integral terms with moments of local accelerations about the particle centroid have also been included in the mathematical framework. The comparison between GEM analysis with and without these terms associated with local acceleration is presented in Fig. 4. The Fig. 4a–d reveal that ignoring influence of local acceleration fields can result in errors up to 5 N in the inter-particle force values in the current granular assembly. Thus ignoring the effect of local acceleration does not have significant impact on the inter-particle forces presented in earlier sections. In [40], the plane stress assumption has been considered in constitutive response but as seen in Fig. 4, the comparison of plane stress and plane strain conditions for same experiment at a particular instant reveals a strong influence of choice of a constitutive law on the inter-particle forces.

Similar trends have been observed for random polycarbonate assembly under impact loading, although the temporal resolution of the impact event is limited due to higher wave velocity for polycarbonate and limitations of image acquisition rates for the camera. Another factor that can have significant influence on the results for a GEM analysis is the accuracy of the constitutive and frictional parameters. In the GEM analysis presented in Fig. 4, nominal values of constitutive constants and frictional coefficients (see Table 1) have been used as inputs. However, it is important to understand the influence of variations in these model parameters on the GEM results.

For the same impact experiment on a randomly arranged polyurethane assembly, inter-particle forces were obtained by employing GEM based analysis for the same experimental strain and kinematics dataset for varying values of Young's modulus E (0.5 $E_{nominal}$ to 1.5 $E_{nominal}$) at nominal frictional coefficient (see Fig. 5). The plots in Fig. 5 clearly indicate that slight variations in Young's modulus do not have a significant impact on the direction of the inter-particle forces. The effect of change in Young's modulus results in an almost proportional change in forces, i.e. 25% change in

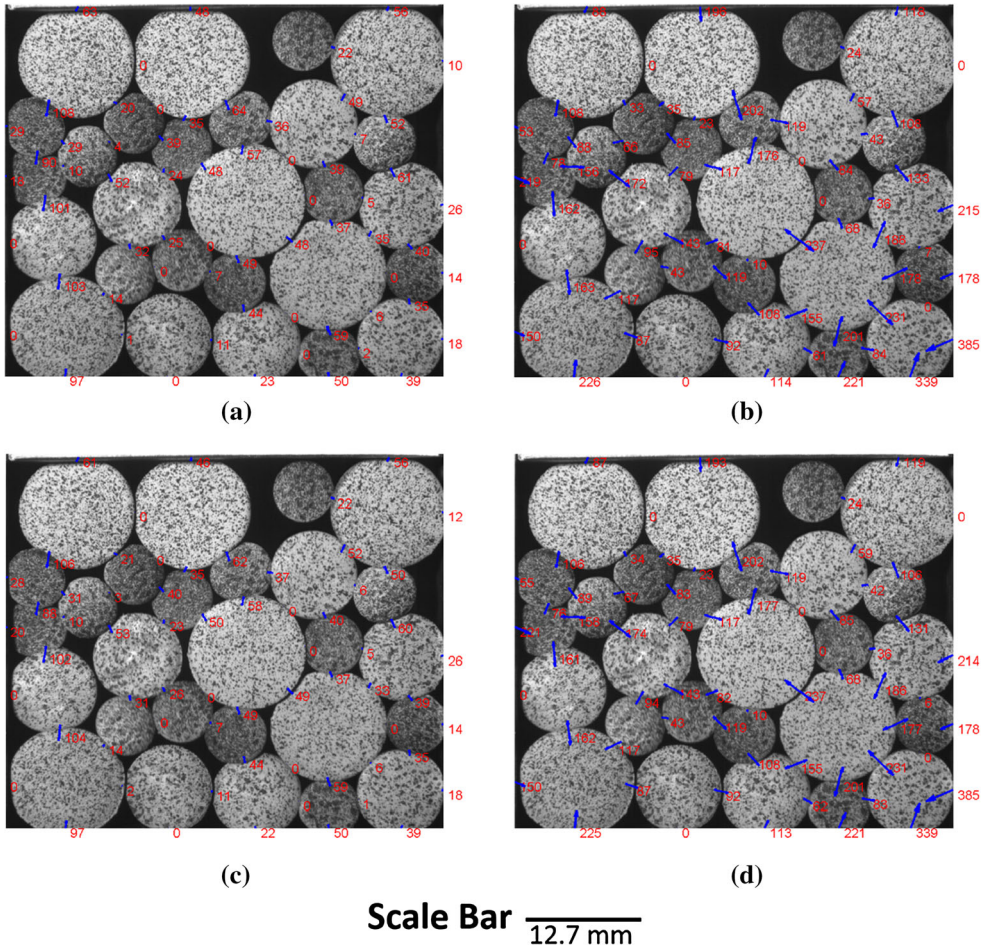

Fig. 4 The inter-particle forces (N) obtained in polyurethane grains using the GEM based approach along with terms accounting for local acceleration fields in each grain for **a** plane stress and **b** plane strain. Inter-particle forces (N) in polyurethane grains ignoring influence of local acceleration fields for **c** plane stress and **d** plane strain at $t = 2$ ms from initial impact

Table 1 Nominal values for constitutive and friction parameters used as input for GEM analysis

	Polycarbonate	Polyurethane
E	2.6 GPa	9.35 MPa
ν	0.37	0.49
μ	0.1	0.5

nominal Young's modulus can result in up to 25–30% change in forces in particles. Thus accurate values of elastic parameters like Young's modulus and Poisson's ratio are important in the calculation of inter-particle forces in granular materials using the GEM approach. However, for the sake of simplicity, the current paper assumes a rate independent linear elastic constitutive law for polyurethane as well as polycarbonate granular particles.

A similar effort was made to investigate the effect of variations in friction coefficient ($\mu = 0$ to $\mu = 1$) for the nominal value for elastic modulus, keeping all other parameters constant (see Fig. 6). The frictional coefficient seems to be more influential on the inter-particle forces obtained by the GEM approach. The frictional coefficient not only influences the magnitude of the inter-particle forces but also the direction of the inter-particle forces in the random polyurethane arrangement. Thus any inaccuracy in the value of the frictional coefficient can have significant implications on the formation of force chains in a larger granular assembly. These trends for variations in the elastic modulus and frictional coefficient also hold for GEM analysis for impact resistant polycarbonate. Since the frictional coefficient seems to have such a significant impact on the inter-particle force measurement by the GEM approach, inter-particle friction between polyurethane–polyurethane, polycarbonate-polycarbonate and polyurethane–polycarbonate surfaces was measured experimentally in this work. This frictional coefficient between two surfaces was measured by the tangential force while sliding a body of known weight with a flat surface over another rigid flat surface. This frictional coefficient

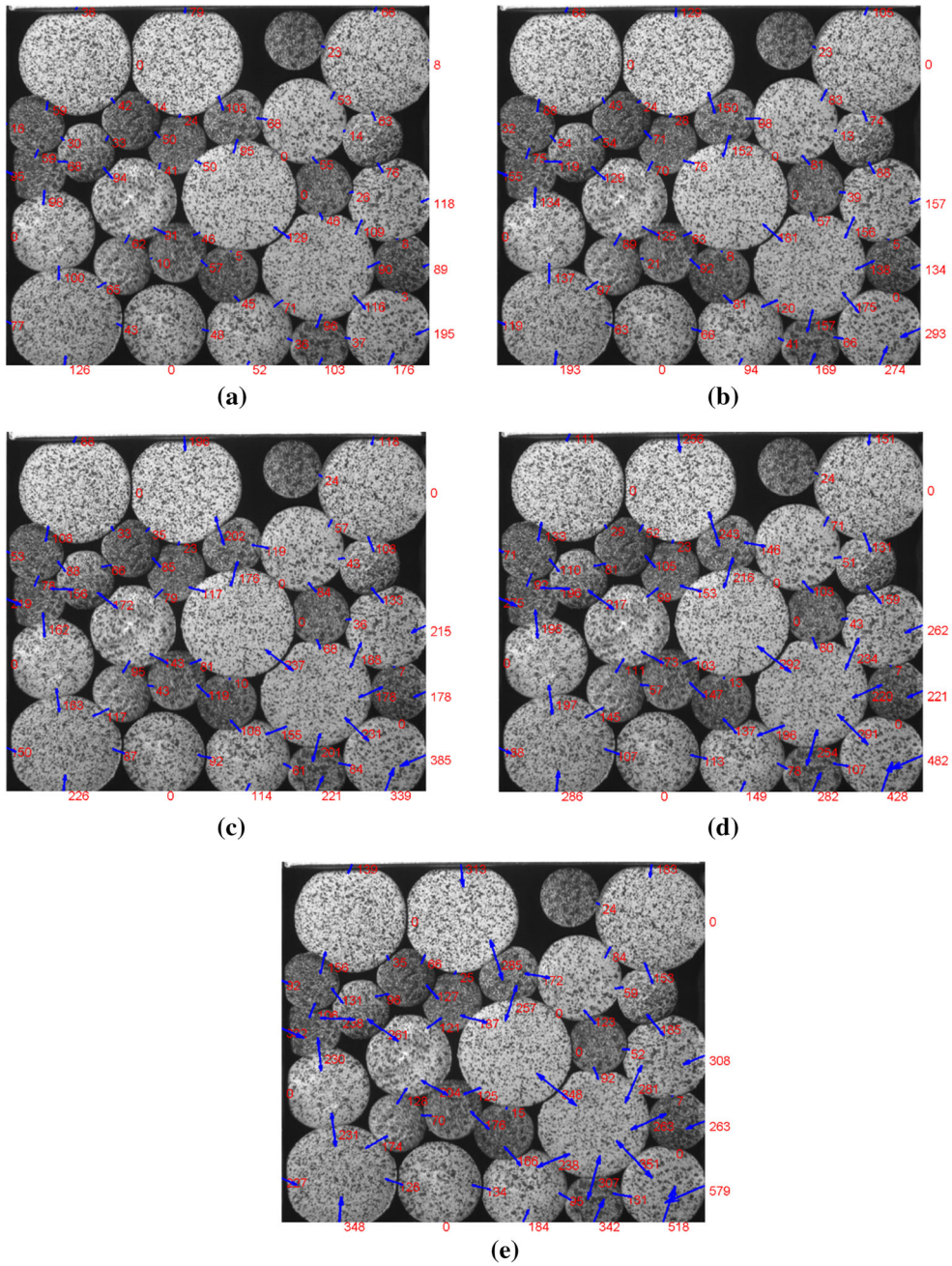

Fig. 5 The inter-particle forces (N) obtained in polyurethane grains using the GEM based approach at time $t = 2$ ms from impact for elastic modulus of **a** *50 %* of $E_{nominal}$, **b** *75 %* of $E_{nominal}$, **c** $E_{nominal}$, **d** *125 %* of $E_{nominal}$ and **e** *150 %* of $E_{nominal}$. The small variations in elastic modulus has no significant impact on the inter-particle forces

was found to be insensitive to sliding velocity within the range investigated (0.01–1 mm/s). The frictional coefficient values measured for these combinations are presented in Table 2.

The monitoring of contribution of different components of energy enhances the understanding of the interaction of particles at the micro-scale and provides means to understand deformation mechanisms at the macro-scale [26–28,41]. The experimental approach developed here facilitates the monitoring of evolution of energy contributions such as elastic energy, frictional losses and kinetic energy in a granular arrangement. The energy entering the system due to impact of the granular assembly with the top wall at any instant t is given by,

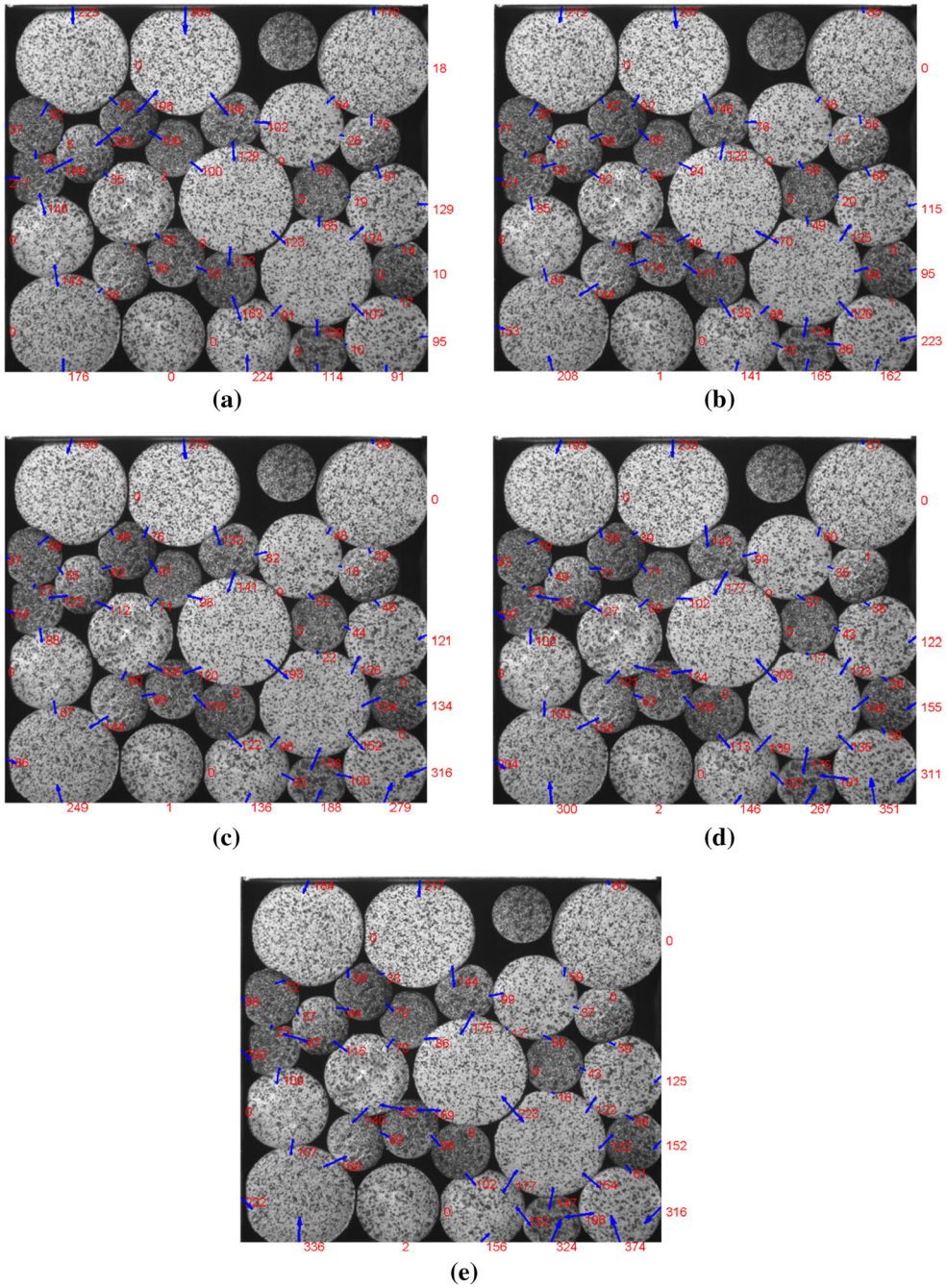

Fig. 6 The inter-particle forces (N) obtained in polyurethane grains at t =1.7 ms using the GEM based approach for frictional coefficient with different values; **a** $\mu = 0$, **b** $\mu = 0.25$, **c** μ, **d** $\mu = 0.75$ and **e** $\mu = 1$

Table 2 The experimentally measured coefficient friction measured for different surfaces

	Polyurethane–Polyurethane	Polyurethane–Polycarbonate	Polycarbonate-Polycarbonate	Polyurethane-Wall	Polycarbonate-Wall
μ	0.43	0.22	0.1	0.25	0.13

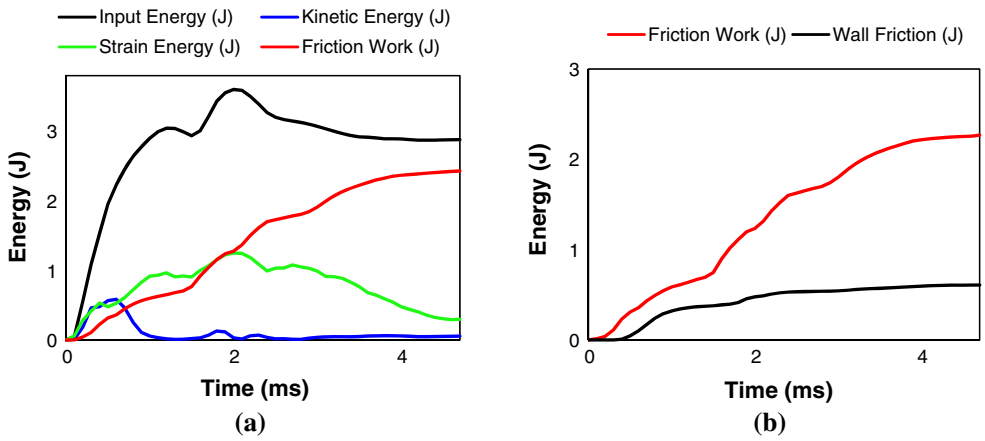

Fig. 7 **a** The evolution of different components of energy and **b** a comparison between wall friction and total work of friction during impact of the random assembly of the polyurethane cylinders

$$E_{in} = \sum_{t=0}^{t} \sum_{i=1}^{N_p} f_i^t \delta u_i \tag{12}$$

where f_i^t is the instantaneous force between particle i and the top wall and δu_i is the corresponding incremental displacement of the top wall. The kinetic energy and the strain energy at any instant is given by,

$$E_{kinetic} = \frac{1}{2} \sum_{p=1}^{N_p} (m_p \dot{u}_p^2 + I_P \omega_p^2) \tag{13}$$

$$E_{strain} = \frac{1}{2} \sum_{p=1}^{N_p} V_p \left(\sigma_{ij} \varepsilon_{ij}\right)_p \tag{14}$$

where m_p is the mass, I_p is moment of inertia and w_p is angular velocity of each particle. Similarly, the GEM approach also allows us to measure the frictional losses at each contact and the energy dissipated through frictional sliding can be obtained using,

$$\begin{aligned} E_{friction} &= \sum_{t=0}^{t} \sum_{i=1}^{N_c} f_{slip}^t \delta u_{slip} \\ &= \sum_{t=0}^{t} \sum_{i=1}^{N_c} (f_i \cdot t_i) \left[(\delta u_i \cdot t_i)_{Grain\,1} \right. \\ &\quad \left. - (\delta u_i \cdot t_i)_{Grain\,2} \right] \end{aligned} \tag{15}$$

where δu_{slip} is the incremental slip displacement vector at the sliding contact for the N_c total contacts at any instant. The contributions of these different energy contributions for the randomly arranged polyurethane assembly is shown in Fig. 7.

As seen in Fig. 7, the input energy representing the transfer of the kinetic energy of the impactor to the granular assembly follows a linear profile and lasted for around 0.5 ms for the random polyurethane assembly. The impactor bounces upwards after initial impact and results in another collision with the sliding top wall granular assembly and results in another smaller increase in the input energy as seen in the Fig. 7. This input energy enters the granular assembly as kinetic energy as evidenced by the high relative contribution of kinetic energy during the initial stages of impact. As the stress wave moves through the granular assembly at a particle velocity around 5 m/s, the contribution of kinetic energy decreases and the elastic strain energy of the system increases correspondingly. The second impact of the impactor with the top wall results in a small burst of kinetic energy and consequently the strain energy reaches its maximum as the granular assembly is compressed. The granular assembly subsequently slowly decompresses as the strain energy of the system is slowly released once again at much slower particle velocity and hence time for strain energy release (∼3 ms) is much larger than time for transfer of initial impact. This energy leaves the system as the kinetic energy of the impactor as the impactor bounces off. Since the impactor is not necessarily in the field of view, it is difficult to account for the kinetic energy of the impactor. Similar analysis for an evolution of energy during impact of a random polycarbonate assembly is shown in Fig. 8. For a random polycarbonate granular assembly, the trends are qualitatively similar but the impact event lasts for much smaller time frame due to higher wave speed. The higher elastic modulus also results in higher relative contribution of the strain energy as compared to polyurethane, however the kinetic energy contribution could possibly increase for granular assemblies with lower packing density, thereby allowing for particle rearrangement. The high relative contribution of frictional losses for both polyurethane and polycarbonate is quite surprising since the magnitude of frictional forces are significantly low ($f_t \sim$ 5–20 N) as compared to normal con-

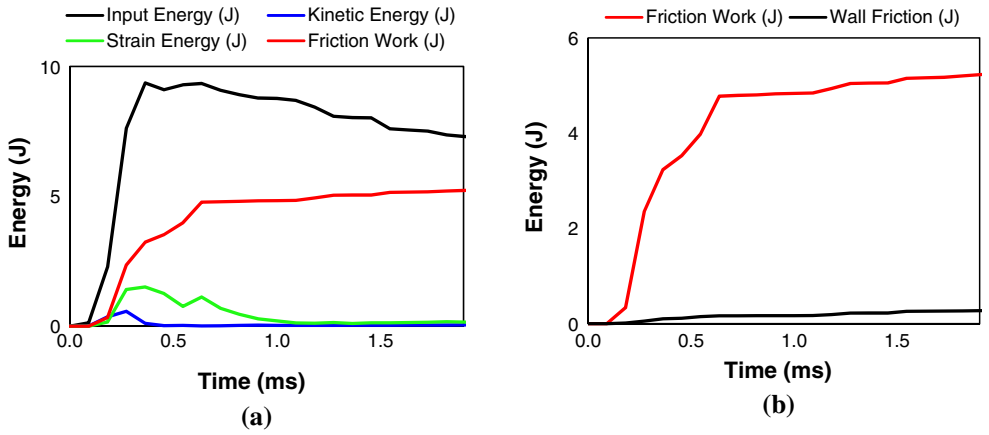

Fig. 8 **a** The evolution of different components of energy and **b** a comparison between wall friction and total work of friction during impact of the random assembly of the polycarbonate cylinders

tact forces which are at least order of magnitude higher at any instant. A closer look at the frictional losses for each contact reveals that the small amount of frictional losses are continually dissipated at each contact over time. It is also noteworthy that contribution of frictional losses at sidewalls and bottom wall in the total work of friction is much lower for the stiffer polycarbonate granular assembly as compared to the polyurethane granular assembly. This is consequence of large strains in polyurethane assembly resulting in large lateral confinement forces against the sidewalls. Thus the large contribution of wall frictional losses in random polyurethane assembly is a direct consequence of the lateral confinement due to the sidewalls and it is likely that the contribution of wall friction in larger granular assembly could be minimal.

In the next section, the utility of the GEM approach is presented through illustrative examples for different packing arrangements. A comparative study of impact loading of different ordered granular packing arrangements for both materials and different particle sizes is presented along with the energy profile for each example.

5 Results

In the first illustration of the GEM approach, two polyurethane particles are subjected to impact loading using the experimental approach presented earlier and the GEM approach is used to obtain the inter-particle forces. The inter-particle force visualization for the impact of two polyurethane cylinders is shown in Fig. 9. A finite-element (FEM) model with the same initial conditions as the experiment was analyzed using ABAQUS-Explicit to compare experimental measurements and results of GEM approach.

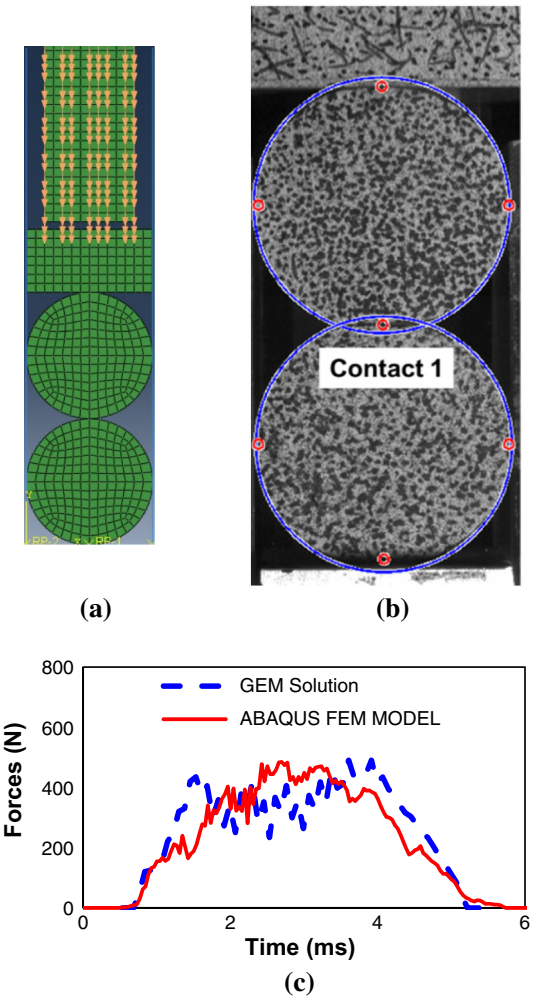

Fig. 9 The schematic for a two particle impact experiment using **a** ABAQUS based FEM simulation and **b** GEM based solution for similar experiment. **c** Comparison between inter-particle forces (N) computed using ABAQUS based FEM simulation and GEM based approach used in the current paper for contact 1 between two particles shown above

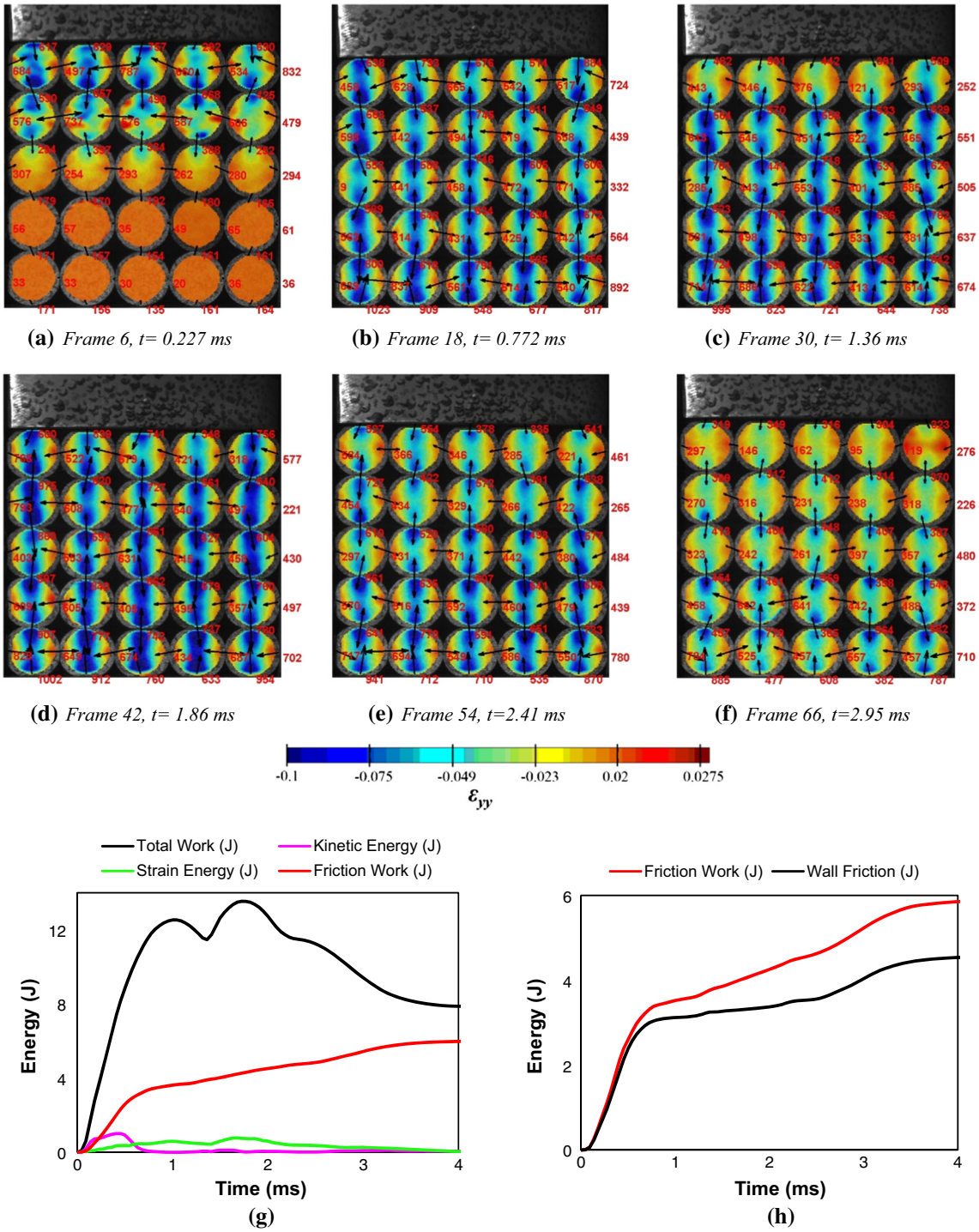

Fig. 10 **a**–**f** The inter-particle forces in BCC ordered polyurethane granular assembly at different instants of time during impact loading calculated using GEM approach. **g** The different components of energy and **h** comparison between wall friction and total work of friction as a function of time for BCC ordered polyurethane granular assembly

The grain material was modeled as 2D plane strain with grain properties for polyurethane discussed in Sect. 4. The walls were modeled as rigid bodies and the impactor was modeled as stiff 2D linear elastic body with material properties for steel. The coefficient of friction between the walls and the grains was experimental measured to 0.22. The comparison between inter-particle forces between two grains using the FEM approach and the GEM analysis for contact 1 is shown in Fig. 9. As seen in Fig. 9, there is reasonable qualitative agreement between the GEM

approach and the FEM simulations for contact 1 during the simple two grain impact experiment. Similar agreement for the inter-particle forces using the two approaches was observed for all the contacts in the 2 particle experiment. The acceleration and strain fields used in the GEM solution during the 2 particle impact experiment was filtered using smoothing functions in the MATLAB while maintaining a signal-to-noise ratio greater than 10 for all the variables. Low-pass filtering of velocity and acceleration data obtained using photo-elasticity experiments with similar signal-to-noise ratio has yielded interesting insight in particle scale dynamics during granular impact [33]. There could be slight differences in the inter-particle forces using the two approaches at certain time instants due to simplifying assumptions in the constitutive and friction laws as well as the effects of the filtering experimental data and experimental errors.

Since the efficacy of the GEM based approach presented in this work has been established through the 2 particle experiment, the utility of the GEM approach is presented to investigate different ordered arrangement of granular assembly. The following ordered granular assemblies of polyurethane and polycarbonate cylinders are presented:

The drop-tower setup introduced in Sect. 3 was employed to apply impact load on a BCC ordered granular assembly of polyurethane cylinders of 3/8″ diameter. The GEM based approach introduced earlier was used to obtain inter-particle forces in BCC polyurethane granular assembly, which are shown in Fig. 10a–f. The large deformation in the polyurethane grains resulted in large lateral strains, ε_{xx} (up to 5%) and which in turn, resulted in large lateral forces (1000 N) due to the confinement effect of the sidewalls. This is also reflected in the large contribution of the wall friction to total frictional losses as the large lateral forces cause significant friction losses. The stress waves move at particle velocities and the stress waves bound around between layers of the granular materials. Similar impact tests on the BCC ordered granular assembly of the stiffer polycarbonate reveals very low contribution of the frictional losses at the sidewalls due to much smaller lateral strains (0.1 %). However, if an external confinement pressure was applied on the stiffer assembly, a similar effect of confinement would be observed.

The velocity in y-direction (direction of impact loading) for each layer of the ordered BCC polyurethane assembly is plotted in Fig. 11, with the top layer being numbered as layer 1 and the successive layers are numbered accordingly. As seen in Fig. 11, the magnitude of initial velocity wave decreases with the successive layers in the granular assembly and the layers are seen to oscillate with the oscillation frequency increasing with successive layers. These oscillations between layers of the granular assembly also leads to lower magnitudes of final velocity in each successive layer.

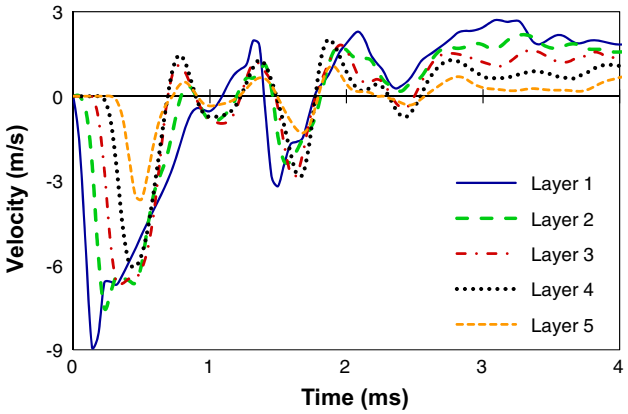

Fig. 11 The velocity in direction of the impact for each layer of the BCC ordered granular assembly of polyurethane cylinders is plotted as a function of time. The layers are sequentially numbered from top to bottom (the top layer numbered as layer 1)

5.1 HCP packed granular assembly

The evolution of inter-particle forces in HCP ordered granular assembly of polyurethane cylindrical particles of 3/8″ diameter using the GEM approach is shown in Fig. 12. As seen in Fig. 12, the large lateral forces (1380 N) are seen due to confinement effects due to the sidewalls and as the result of the large lateral strains (ε_{xx} up to 4.5%) and lateral motion as a result of the contacts being at the 45° angle to the direction of the vertical impact loading. The contact angle with respect to the direction of loading in the HCP granular assembly also results in higher frictional forces in polyurethane assembly. As seen in Fig. 12, the wall friction is much lower in HCP granular assembly compared to BCC ordered granular assembly as only half the layers in the HCP are in contact with the sidewalls. However, in spite of significantly lower magnitude of wall friction, the frictional losses in HCP assembly lead to better frictional dissipation in the HCP granular assembly in comparison with the BCC assembly. The evolution of different components of energy for HCP granular assembly is shown in Fig. 12g and the contribution of the strain energy is much higher in HCP granular assembly compared to the BCC assembly due to higher packing density. The kinetic energy in the HCP granular assembly is also lower than the BCC assembly to the direction of the contact angle with respect to the applied impact loading resulting in much larger lateral constraints and in loss of kinetic energy due to frictional losses.

This effect of larger lateral constraints is also reflected when the velocity of the granular layers in the HCP assembly in the direction of impact loading is plotted in Fig. 13. As seen in Fig. 13, the average velocity in vertical direction for the HCP granular assembly is significantly lower than the BCC assembly for each layer due to angle of con-

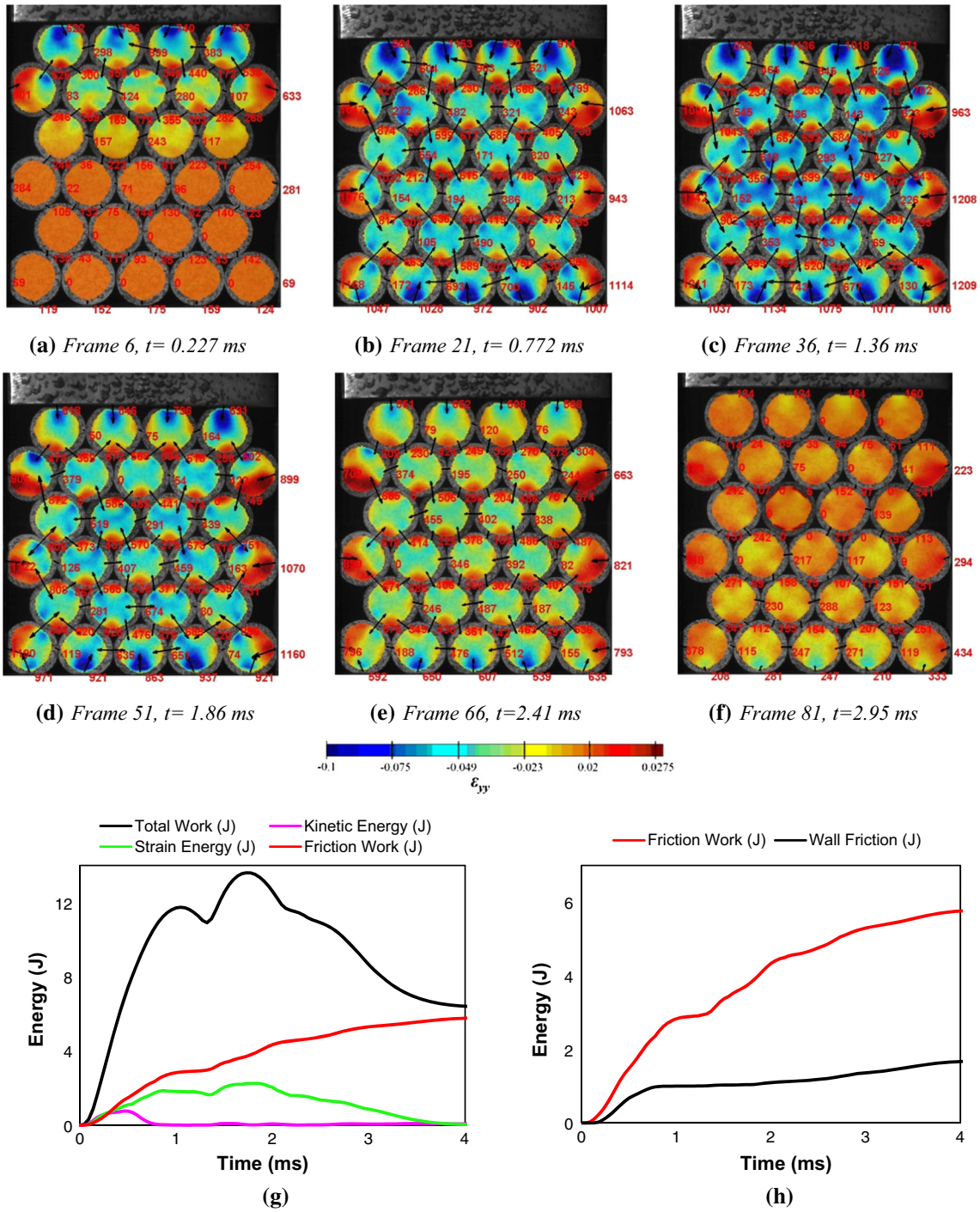

Fig. 12 **a**–**f** The inter-particle forces in HCP ordered polyurethane granular assembly at different instants of time during impact loading calculated using GEM approach. **g** The different components of energy and **h** comparison between wall friction and total work of friction as function of time for HCP ordered polyurethane granular assembly

tacts with respect to direction of loading. Similar to the BCC granular assembly, the magnitude of initial velocity wave decreases with the successive layers in the granular assembly and the layers are seen to oscillate with the oscillation frequency increasing with successive layers. The velocity profile of layer 6 reflects that the vertical velocity dissipates within a very short time interval after arrival of initial wave and seems to follow similar trend upon the arrival of second impact pulse. The grains in densely packed ordered BCC and HCP granular assembly undergo little to no grain rotation and

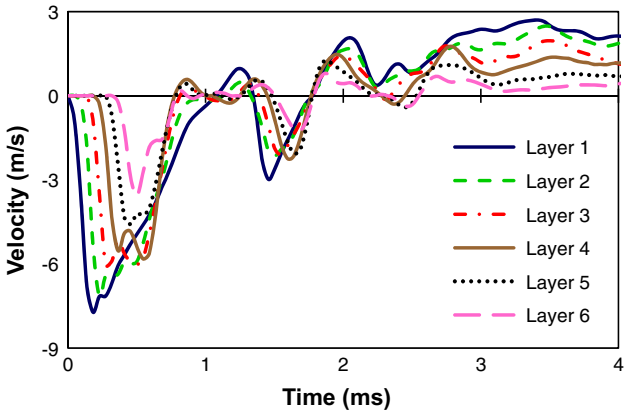

Fig. 13 The velocity in direction of the impact for each layer of the HCP ordered granular assembly of polyurethane cylinders is plotted as a function of time. The layers are sequentially numbered from *top* to *bottom* (the top layer numbered as layer 1)

shear banding under impact loading in the current work. The contribution of rotational energy to total kinetic energy of the system is minimal in the experiments presented in this work.

5.2 HCP packed granular assembly with a void

The evolution of inter-particle forces in HCP ordered granular assembly of polyurethane cylindrical particles of 3/8″ diameter with a void using the GEM approach is shown in Fig. 14. Although the maximum lateral forces in the HCP granular assembly with a void have similar values (∼1300 N) as the lateral forces in the HCP granular assembly in the last section. However, these maximum lateral forces occur in the Layer 2 that are the above the void in the assembly. The maximum lateral forces in the layer 4 (layer with the void) are much lower around 900 N. This is rather expected since the void in the layer 4 allows for the relaxation of the lateral constraints and resulting in lower lateral forces. These lower values of lateral forces lead to decrease in frictional losses due to wall friction as compared to the HCP granular assembly. There is significant wave scattering around the void and the inter-particle forces around the void were also greatly elevated. These observations are consistent with the dynamic photo-elasticity experiments by Shukla [5].

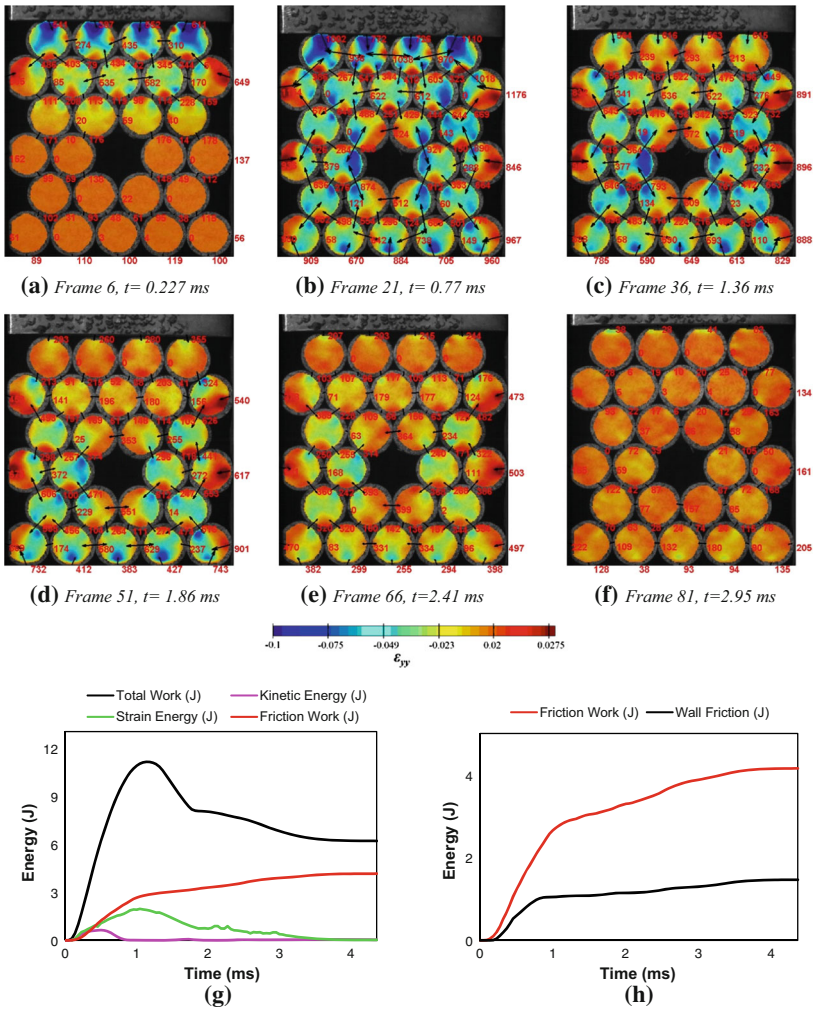

Fig. 14 **a**–**f** The inter-particle forces in HCP ordered polyurethane granular assembly with a void at different instants of time during impact loading calculated using GEM approach. **g** The different components of energy and **h** comparison between wall friction and total work of friction as function of time for HCP ordered polyurethane granular assembly with a void

The vertical velocity of the different layers in HCP granular assembly with a void is plotted in Fig. 15, with the top layer being numbered as layer 1 and the layer 4 has a void along the centerline of the impact loading direction. As seen in Fig. 15, there is significant drop in vertical velocity from the Layer 3 to Layer 4 as well as Layer 4

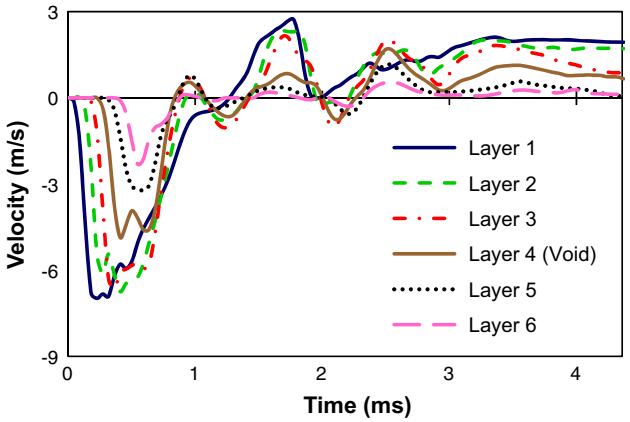

Fig. 15 The velocity in direction of the impact for each layer of the HCP ordered granular assembly of polyurethane cylinders with a void is plotted as a function of time. The layers are sequentially numbered from *top* to *bottom* (the top layer numbered as layer 1)

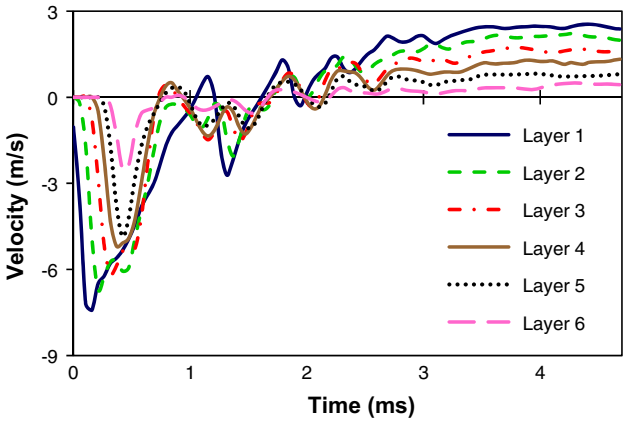

Fig. 17 The velocity in direction of the impact for each layer of the BCC–BCC layered polyurethane granular assembly is plotted as a function of time. The layers are sequentially numbered from *top* to *bottom* (the top layer numbered as layer 1)

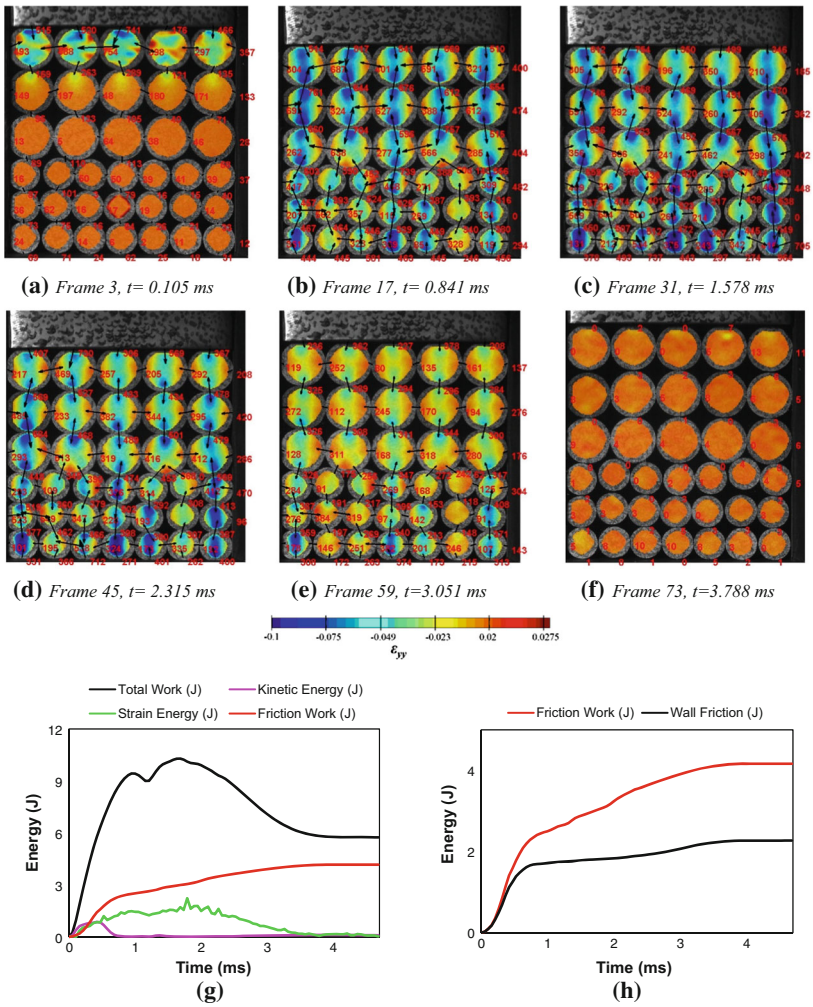

Fig. 16 **a**–**f** The inter-particle forces in BCC–BCC layered polyurethane granular assembly at different instants of time during impact loading calculated using GEM approach. **g** The different components of energy and **h** comparison between wall friction and total work of friction as function of time for BCC–BCC layered polyurethane granular assembly

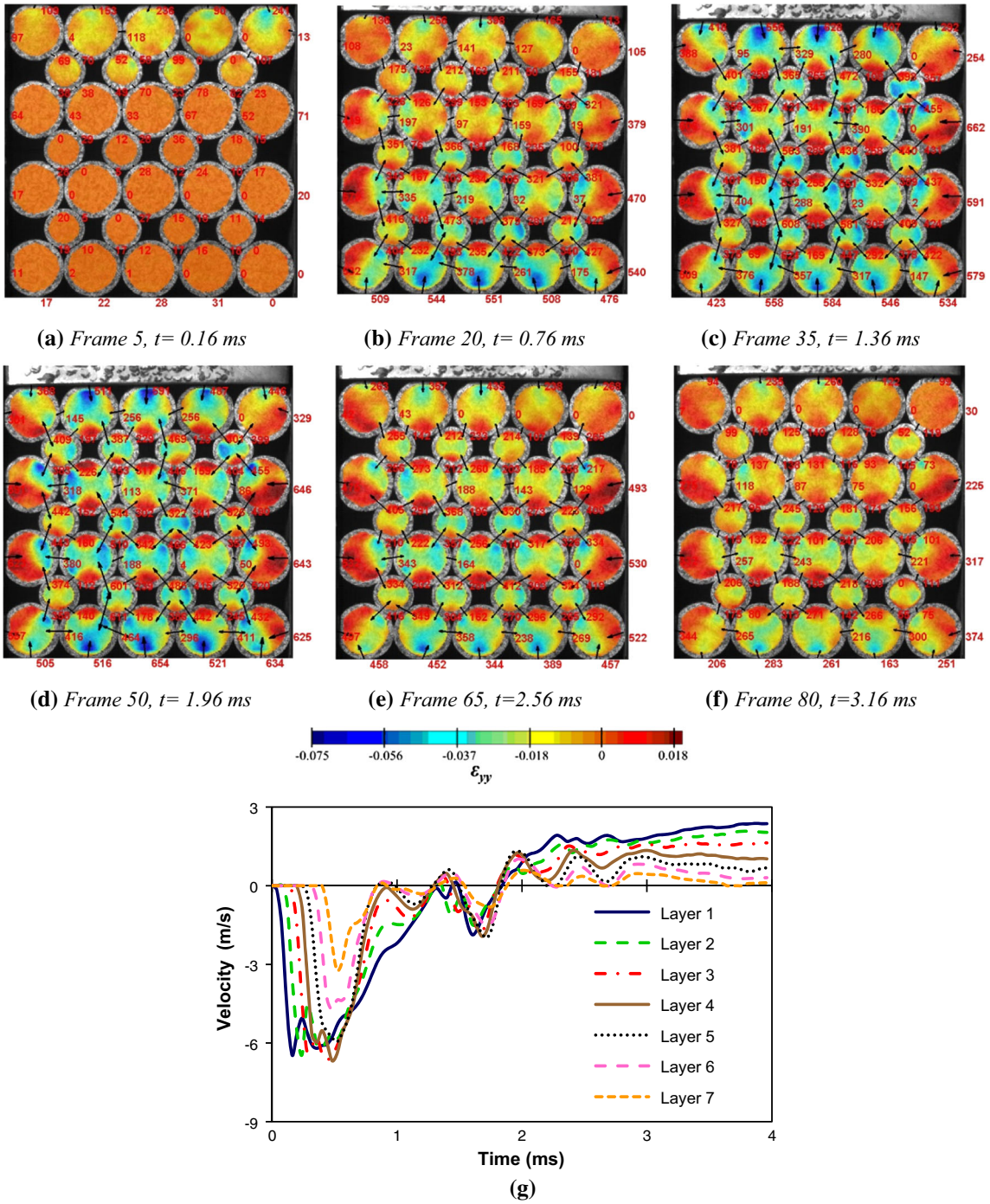

Fig. 18 a–f The inter-particle forces in HCP-HCP layered polyurethane granular assembly at different instants of time during impact loading calculated using GEM approach. The velocity in direction of the impact for each layer of the HCP-HCP layered polyurethane granular assembly is plotted as a function of time. The layers 2, 4, 6 are polyurethane cylinders with 1/4″ diameter while layers 1, 3, 5, 7 are polyurethane cylinders with 3/8″ diameter

to Layer 5. Thus the presence of a void results in significant attenuation around it and it also resulted in lowering the oscillations in the granular assembly. However, the far field effect of the presence of void in HCP granular assembly is not clearly studied in this work as the lateral confinement effects due to the walls may significantly affect the dynamic load transfer in the granular assembly.

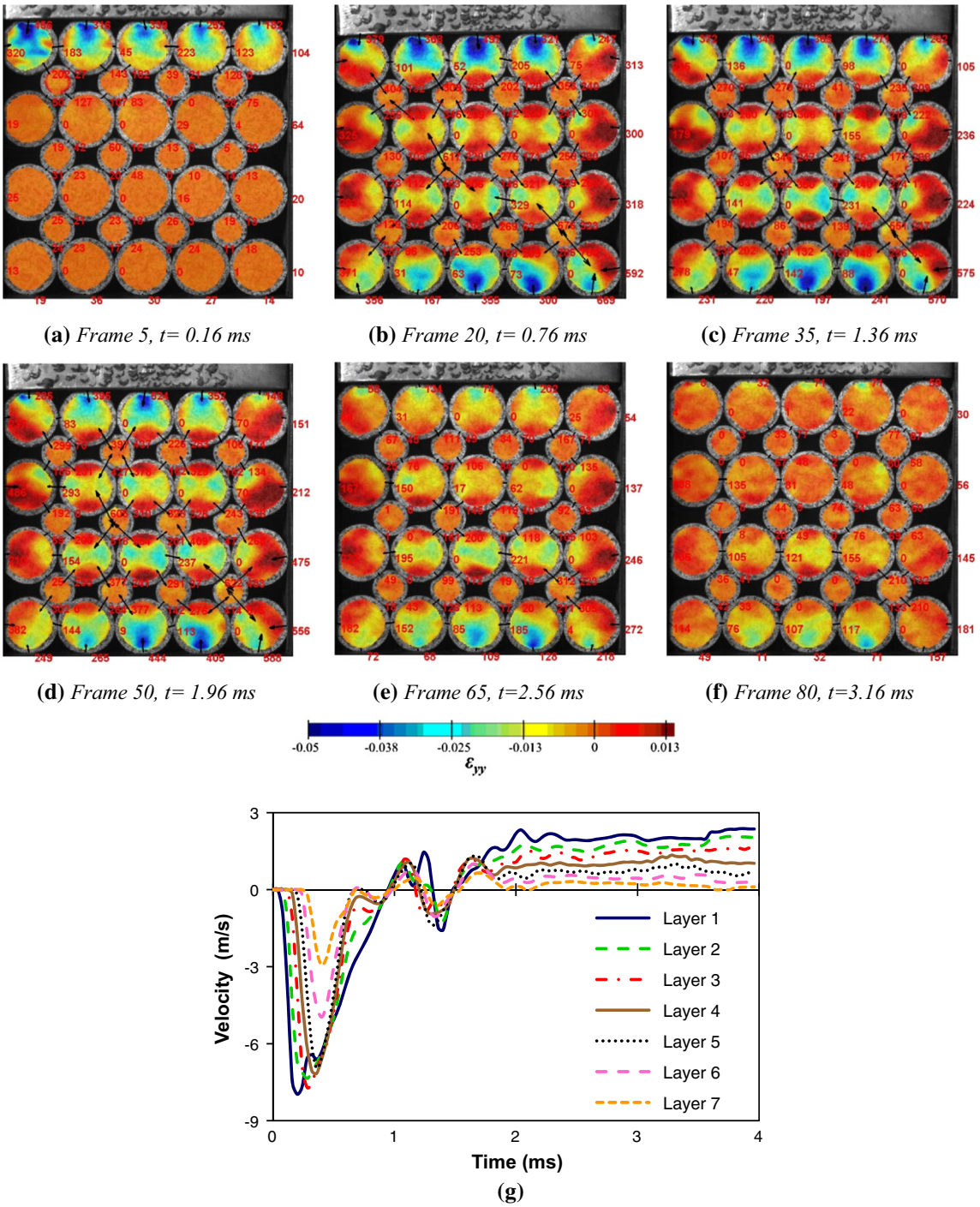

Fig. 19 **a–f** The inter-particle forces in HCP layered polyurethane–polycarbonate granular assembly at different instants of time during impact loading calculated using GEM approach. **g** The velocity in direction of the impact for each layer of the HCP-HCP layered polyurethane granular assembly is plotted as a function of time. The layers 2, 4, 6 are polycarbonate cylinders with 1/4″ diameter while layers 1, 3, 5, 7 are polyurethane cylinders with 3/8″ diameter

5.3 Layered BCC–BCC granular assembly

In this granular assembly, the Layers 1–3 consisted of a BCC arrangement with 3/8″ diameter polyurethane cylinders while Layers 4–6 consisted of a BCC arrangement with 1/4″ diameter polyurethane cylinders. The evolution of inter-particle forces in this layered assembly under vertical impact loading is shown in Fig. 16. Due to the non-uniform interface

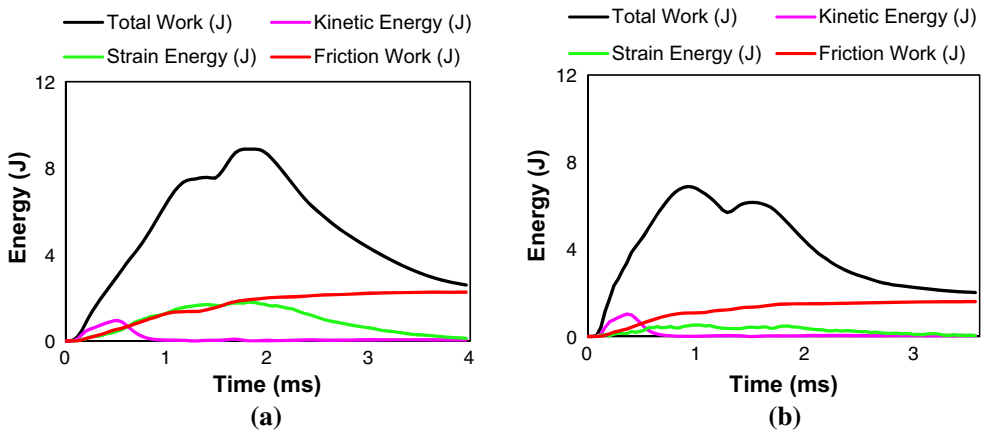

Fig. 20 A comparison between different components of energy in **a** bi-disperse polyurethane layered assembly and **b** bi-disperse polycarbonate and polyurethane assembly

between layer 3 and layer 4, layers 4–6 do not necessarily behave as an ordered BCC granular assembly and these layers are deformed asymmetrically and hence result in much larger lateral forces than observed in layers 1–3. These lateral forces are highly asymmetrical, i.e. the lateral forces in any of the layers 4–6 against the right and left wall are significantly different. The exact extent of the asymmetry caused by such a non-uniform interface cannot be determined in the current work and would require the investigation of a much larger granular assembly.

The vertical velocity for the different layers in BCC–BCC granular assembly is plotted in Fig. 17, with the top layer being numbered as layer 1. As seen in Fig. 17, the vertical velocity decreases significantly for layers 4–6 and the frequency and the amplitude of oscillations is also lower for these layers. The velocity profile of layer 6 reflects that the vertical velocity dissipates within a very short time interval after arrival of initial wave.

5.4 Layered HCP granular assembly

In this section, the impact response of two types of layered HCP granular assemblies are compared using the GEM approach. The first granular assembly in this section is a HCP- HCP bi-disperse polyurethane layered assembly where the layers 2, 4, 6 are polyurethane cylinders with 1/4″ diameter while layers 1, 3, 5, 7 are polyurethane cylinders with 3/8″ diameter (top layer is numbered as layer 1). The evolution of inter-particle forces in this layered assembly under vertical impact loading is shown in Fig. 18. The Fig. 18 also shows the velocity in direction of the impact for each layer of the HCP-HCP layered polyurethane granular assembly as a function of time. A closer look at velocity profiles for layers 1, 2, 3, 4 in Fig. 18f reveal significant oscillations in the waves around the first velocity peak. The wave oscillations indicate successive collisions between the HCP layers since there is approximate 180° phase difference between layers 1 and 2. These successive collisions also result in significant broadening of the waves (Fig. 18f).

The second granular assembly in this section is a HCP-HCP polyurethane–polycarbonate layered assembly where the layers 2, 4, 6 are polycarbonate cylinders with 1/4″ diameter while layers 1, 3, 5, 7 are polyurethane cylinders with 3/8″ diameter (top layer is numbered as layer 1). The evolution of inter-particle forces in this layered polyurethane–polycarbonate assembly under vertical impact loading along with the vertical velocity for different layers as function of time are shown in Fig. 19. These plots clearly show how the polyurethane assembly deforms uniformly while the polyurethane–polycarbonate assembly deforms in the heterogeneous manner as the stiffer polycarbonate layers almost act as a rigid particles under impact loading. Expectedly, the vertical velocity of the layers is significantly higher in the polycarbonate-polyurethane assembly due to the higher wave speed in the stiffer polycarbonate material. The comparison between layer velocities for both assemblies indicate the amplitude of oscillations is much higher for polycarbonate-polyurethane assembly. However, the oscillations in the polyurethane–polycarbonate mixture dissipate much faster while the poly-disperse polyurethane assembly keeps oscillating for a much longer time. A comparison between the different energy components for two types of layered granular assemblies is presented in Fig. 20. The input energy in two layered assemblies compare well till the first peak and there is significant deviation beyond this point. The total energy of bi-disperse polyurethane assembly follows a similar qualitative profile to the cases presented in earlier sections. In contrast, the total energy of the polyurethane–polycarbonate assembly actually decreases after the first peak as some of energy entering the system during the first impact may have been reflected from different polyurethane–polycarbonate interfaces. The acoustic

impedance mismatch at these interfaces could result in significant wave reflections and the stiffer polycarbonate results in this energy reflection to occur before the second impact. As expected, the strain energy contribution in the polyurethane layered assembly is much larger than the polyurethane–polycarbonate assembly. These initial observations seem to suggest that layered bi-material granular assembly such as the polyurethane–polycarbonate mixture here would be more suited to dissipation impact loading and could prove as candidate materials for applications involving impact mitigation or shock protection.

6 Conclusions

The utility of the granular element method based mathematical framework to infer inter-particle forces in granular materials is demonstrated in the current work. The mathematical framework is presented along with an analysis of the sensitivity of different input parameters such as coefficient of friction, constitutive law for individual grains and elastic modulus. It was observed that assumption of the constitutive law (plane stress Vs plane strain) as well as the changes in modulus significantly affect the magnitude of the inter-particle forces using the GEM approach while the friction coefficient affects both the magnitude and direction of the inter-particles and thus can influence the predictions of the formation of force chains in the granular assembly. The inter-particle forces computed using the GEM approach for a simple 2 particle granular assembly under impact loading show good agreement with the predictions for inter-particle forces using an idealized ABAQUS explicit based FEM model. Since the experimental approach in this work provides high fidelity full-field strain and kinematic measurements and accurate predictions of inter-particle forces using GEM, it provides a great opportunity to monitor the contribution of different components of energy such as kinetic energy, strain energy, work of friction and the energy exchange with the surroundings through the moving top wall.

The GEM based methodology is used to investigate the mechanical response of different ordered granular assemblies under impact loading. However, the results in the current work exhibit significant influence of the confinement effects due to small system size and the high lateral forces experienced by the assemblies due to sidewalls. It is also noteworthy that although the frictional forces between particles in the granular assemblies are relatively small, the frictional dissipation due to the inter-particle forces plays a major role in impact response of granular materials. The investigation of ordered granular assembly with void under impact loading indicated that local inter-particle forces near the void were significantly elevated and the presence of the void caused significant wave scattering and attenuation. Thus the GEM analysis indicated the presence of defects can have significant influence on the wave propagation in the granular assemblies. This work also investigates the impact response of different layered granular assemblies which have effective dissipative response to impact waves.

Acknowledgements The author would like to acknowledge his collaborators G. Ravichandran and J. Andrade at California Institute of Technology for their fruitful discussions and support in development of GEM based analysis. The author would also like to acknowledge the support by DTRA Award No. HDTRA1-12-1-0041.

Compliance with ethical standards

Conflict of interest No potential conflict of interest is reported by the author. None of the material presented in the paper is submitted or published elsewhere, and the paper does not contain any information with restricted access or proprietary content

References

1. Dantu, P.: Statistical study of intergranular forces in a powdery medium. Geotechnique **18**, 50–55 (1968)
2. Behringer, R., Howell, D., Kondic, L., Tennakoon, S., Veje, C.: Predictability and granular materials. Phys. D Nonlinear Phenom. **133**, 1–17 (1999)
3. Geng, J., Reydellet, G., Clément, E., Behringer, R.P.: Green's function measurements of force transmission in 2D granular materials. Phys. D Nonlinear Phenom. **182**, 274–303 (2003)
4. Majmudar, T.S., Behringer, R.P.: Contact force measurements and stress-induced anisotropy in granular materials. Nature **435**, 1079–1082 (2005)
5. Shukla, A.: Dynamic photoelastic studies of wave propagation in granular media. Opt. Lasers Eng. **14**, 165–184 (1991)
6. Lesniewska, D., Wood, D.M.: Observations of stresses and strains in a granular material. J. Eng. Mech. **135**, 1038–1054 (2009)
7. Bouchaud, J.P., Claudin, P., Levine, D., Otto, M.: Force chain splitting in granular materials: a mechanism for large-scale pseudo-elastic behaviour. Eur. Phys. J. E **4**, 451–457 (2001)
8. Herrmann, H.J., Luding, S.: Modeling granular media on the computer. Continuum Mech. Thermodyn. **10**, 189–231 (1998)
9. Peters, J.F., Muthuswamy, M., Wibowo, J., Tordesillas, a: Characterization of force chains in granular material. Phys. Rev. E Stat. Nonlinear Soft Matter. Phys. **72**, 1–8 (2005)
10. Bourrier, F., Nicot, F., Darve, F.: Physical processes within a 2D granular layer during an impact. Granul. Matter. **10**, 415–437 (2008)
11. Jensen, R.P., Bosscher, P.J., Plesha, M.E., Edil, T.B.: DEM simulation of granular media-structure interface: effects of surface roughness and particle shape. Int. J. Numer. Anal. Methods Geomech. **23**, 531–547 (1999)
12. Cundall, P.A., Strack, O.D.L.: A discrete numerical model for granular assemblies. Géotechnique **29**, 47–65 (1979)
13. Dafalias, Y.F., Popov, E.P.: A model of nonlinearly hardening materials for complex loading. Acta Mech. **21**, 173–192 (1975)
14. DiMaggio, F.L., Sandler, I.S.: Material model for granular soils. J. Eng. Mech. Div. **97**, 935–950 (1971)
15. Andrade, J.E., Borja, R.I.: Capturing strain localization in dense sands with random density. Int. J. Numer. Methods Eng. **67**, 1531–1564 (2006)
16. Nedderman, R.M.: Statics and Kinematics of Granular Materials. Cambridge University Press, Cambridge (1992)

17. Goldenberg, C., Goldhirsch, I.: Friction enhances elasticity in granular solids. Nature **435**, 188–191 (2005)
18. Savage, S.B.: Modeling and granular material boundary value problems. In: Herrmann, H.J., Hovi, J.-P., Luding, S. (eds.) Physics of Dry Granular Media, pp. 25–95. Springer, Dordrecht (1998)
19. Wu, W., Bauer, E., Kolymbas, D.: Hypoplastic constitutive model with critical state for granular materials. Mech. Mater. **23**, 45–69 (1996)
20. Drescher, A., de Josselin de Jong, G.: Photoelastic verification of a mechanical model for the flow of a granular material. J. Mech. Phys. Solids **20**, 337–340 (1972)
21. Christoffersen, J., Mehrabadi, M.M., Nemat-Nasser, S.: A micromechanical description of granular material behavior. J. Appl. Mech. **48**, 339 (1981)
22. Bathurst, R.J., Rothenburg, L.: Observations on stress-force-fabric relationships in idealized granular materials. Mech. Mater. **9**, 65–80 (1990)
23. Chang, C.S., Ma, L.: A micromechanical-based micropolar theory for deformation of granular solids. Int. J. Solids Struct. **28**, 67–86 (1991)
24. Somfai, E., Roux, J.-N., Snoeijer, J., van Hecke, M., van Saarloos, W.: Elastic wave propagation in confined granular systems. Phys. Rev. E **72**, 21301 (2005)
25. Pal, R.K., Geubelle, P.H.: Wave tailoring by precompression in confined granular systems. Phys. Rev. E **90**, 1–9 (2014)
26. Morgado, W.a M., Oppenheim, I.: Energy dissipation for quasielastic granular particle collisions. Phys. Rev. E **55**, 1940–1945 (1997)
27. Shamy, U.El, Denissen, C.: Microscale energy dissipation mechanisms in cyclically-loaded granular soils. Geotech. Geol. Eng. **30**, 343–361 (2012)
28. Pal, R.K., Geubelle, P.H.: Impact response of elasto-plastic granular and continuum media: a comparative study. Mech. Mater. **73**, 38–50 (2014)
29. Cates, M., Wittmer, J., Bouchaud, J.-P., Claudin, P.: Jamming, force chains, and fragile matter. Phys. Rev. Lett. **81**, 1841–1844 (1998)
30. O'Hern, C.S., Langer, S.A., Liu, A.J., Nagel, S.R.: Force distributions near jamming and glass transitions. Phys. Rev. Lett. **86**, 111–114 (2001)
31. van Hecke, M.: Jamming of soft particles: geometry, mechanics, scaling and isostaticity. J. Phys. Condens. Matter. **22**, 33101 (2010)
32. Pica Ciamarra, M., Lara, A.H., Lee, A.T., Goldman, D.I., Vishik, I., Swinney, H.L.: Dynamics of drag and force distributions for projectile impact in a granular medium. Phys. Rev. Lett. **92**, 194301 (2004)
33. Clark, A.H., Kondic, L., Behringer, R.P.: Particle scale dynamics in granular impact. Phys. Rev. Lett. **109**, 238302 (2012)
34. Nesterenko, V.F.: Dynamics of Heterogeneous Materials. Springer, New York, NY (2001)
35. Sanchez, M., Carlevaro, C.M., Pugnaloni, L.A.: Effect of particle shape and fragmentation on the response of particle dampers. J. Vib. Control **20**, 846–1854 (2013)
36. Howell, D., Behringer, R., Veje, C.: Stress fluctuations in a 2D granular Couette experiment: a continuous transition. Phys. Rev. Lett. **82**, 5241–5244 (1999)
37. Saadatfar, M., Sheppard, A.P., Senden, T.J., Kabla, A.J.: Mapping forces in a 3D elastic assembly of grains. J. Mech. Phys. Solids **60**, 55–66 (2012)
38. Zhou, J., Long, S., Wang, Q., Dinsmore, A.D.: Measurement of forces inside a three-dimensional pile of frictionless droplets. Science **312**, 1631–1633 (2006)
39. Hurley, R., Marteau, E., Ravichandran, G., Andrade, J.E.: Extracting inter-particle forces in opaque granular materials: beyond photoelasticity. J. Mech. Phys. Solids **63**, 154–166 (2014)
40. Hurley, R.C., Lim, K.W., Ravichandran, G., Andrade, J.E.: Dynamic inter-particle force inference in granular materials: method and application. Exp. Mech. **56**, 217–229 (2016)
41. Babic, M.: Average balance equations for granular materials. Int. J. Eng. Sci. **35**, 523–548 (1997)